Crystallization of D_2O thin films on Ru(001) surfaces

T. Yamauchi, K. Mine, Y. Nakashima, A. Izumi, A. Namiki*

Department of Electrical Engineering and Electronics,

Kyushu Institute of Technology, Kitakyushu, Japan.

(Dated: January 26, 2009)

Abstract

The phase conversion of amorphous solid water (ASW) to crystalline ice (CI) has been investigated in the very thin ($\sim$ 10 monolayers) film regime on a Ru(001) surface. We analyze the converted CI fraction with the Avrami model, and recognize that one dimensional CI growth occurs, which can be contrasted to the three dimensional CI growth generally established in the thick ($\geq$ 50 monolayers) film regime. We evaluate activation energy for the ASW crystallization to be about 1.0 eV. We suggest that the ASW crystallization is not influenced by the substrate even near the substrate-ice interface.

PACS numbers: 33.20.Ea, 87.15.nt

*Electronic address: yamauchi@ele.kyutech.ac.jp(T.Yamauchi)

keywords : Ruthenium; Crystallization; Amorphous solid water; Infrared spectrum

I. INTRODUCTION

Water ice has accumulated interests particularly in the field of astrophysics. Astronomers consider that interstellar hydrogen molecules, from which a new star is born in molecular clouds, are synthesized via recombination of H atoms at surfaces of non crystalline, amorphous solid water (ASW) mantling fine dust grains [1, 2]. The ASW surfaces also provide vital reaction sites for photo- or cosmic ray-synthesis of molecules such as CO and CO_2 [3], which are indeed recognized in the ASW layers of such ice mantles [4].

ASW is known to take different structural phases depending on preparation conditions such as annealing or deposition temperature. ASW is formed as solid surfaces are exposed to water molecules at temperatures below $\sim$130 K and it is converted to crystalline ice (CI) by thermal annealing above 135 K [5, 6]. Kinetics of ASW crystallization have been extensively studied by means of nondestructive methods such as isothermal temperature programmed desorption (ITPD) (also including linear temperature rise) [7–12] and reflection infrared absorption spectroscopy (IRAS) [13–16]. At temperatures typical for ASW crystallization the sublimation rate is larger on ASW than on CI [17]. Hence ITPD curves measured during crystallization include a burst like peak, being attributed to the molecular desorption from ASW. Such a burst of molecular emission is generally followed by a nearly linear, slow decay of ITPD, attributable to sublimation of converted CI [7]. So far, on the basis of such desorption data, kinetics of ASW crystallization have been elucidated on various substrates. For ASW as thick as 50 monolayers (ML), spatially as well as temporally random nucleation followed by isotropic CI growth was suggested to generally occur in the bulk of ASW rather than at its surface or the substrate-ice interface. Kondo et al. [13–15] confirmed it

more directly by means of He atom scattering combined with IRAS and ITPD on Ru(001) surfaces.

For ASW much thinner than 50 ML, on the other hand, it was found that ASW crystallization rate become faster, which could be categorized to phase conversion at the substrate-ice interface [18]. However, compared with ASW crystallization in the thick film regime, only a little is known about kinetic mechanism of the ASW crystallization in the thin film regime below 25 ML. In this work, employing IRAS combined with ITPD we investigate ASW crystallization process in a thin film regime for 8-25 ML D_2O layers on a Ru(001) surface.

II. EXPERIMENT

The experiments were conducted in an ultrahigh vacuum chamber (base pressure of 1×10^{-8} Pa) equipped with an Auger electron spectrometer AES, two quadrupole mass spectrometers (QMS1 and QMS2 for a angle resolved and integrated mode, respectively), Fourier transformed infrared light (FT-IR) optics for IRAS, an Ar^+ ion sputter gun, and a flow type liquid N_2 cryostat. The FT-IR lights are p-polarized and focused on the sample surface by a concave mirror through a BaF viewport at an 85° grazing angle of incidence to the sample surface. The IR light reflected from the surface was detected by a mercury-cadmium-telluride detector through another BaF viewport. The path of the IR lights and the mirror system outside the UHV chamber were evacuated below 133 Pa with a rotary pump. This evacuation of the FT-IR system could minimize the influence of background gases such as H_2O and CO_2, thus improving S/N ratios of IRAS spectra of a OD stretching mode at the region from 2200 to 2700 cm^{-1}. A reference spectrum for the IRAS spectra was obtained on a clean Ru(001) surface prior to D_2O deposition. IRAS spectra of the OD stretching mode were recorded after averaging of 8 scans (10 s) with a 4 cm^{-1} spectral resolution. A Ru(001)

single crystal (diameter: 10 mm, thickness: 2 mm) was spot welded to a tantalum plate, which was attached to a copper holder packing a sapphire plate for electrical insulation but thermal conduction from the cryostat. The copper holder was equipped with the sample heating system by means of electron bombardment. A K-type thermocouple was spot welded to the side of the sample disc. The Ru(001) surface was cleaned by cycles of 1 keV Ar^+ ion sputtering at 300 K, combined with ashing of C contaminants with O_2 gas at 1000 K in UHV chamber. We confirmed no presence of O and C adatoms on the surface in the AES spectrum. Deionized D_2O water was treated by repeated freez-pump- thaw cycles to degas extraly resolved gases. The vessel of D_2O water was then applied by 5 Pa He gas. The D_2O ice layers were formed by dosing water vapor through a 1 mm capillary doser onto the clean Ru(001)surface at 84 K. Water dose was monitored by the He peak measured with the QMS signals. Typical deposition rate was 0.1 ML/s. However, its regulation was a bit poor and therefore the thickness of the deposited films was spread in the range from 8-25 ML. The substrate temperature was increased from 84 K to desired crystallization temperature (147, 148, 149, 150 and 152 K) with a heating rate of 0.2 K/s. During annealing process IRAS spectra of the OD stretching mode and QMS spectra of mass 18 were recorded to analyze ASW crystallization.

III. RESULTS AND DISCUSSION

IRAS spectra were measured during ASW crystallization and CI sublimation at temperatures of 147, 148, 149, and 150 K. The IRAS spectrum for ASW had a main peak at 2550 cm^{-1} and weak shoulders at around 2450 and 2350 cm^{-1}. On the other hand, the IRAS spectrum for CI had a main peak at 2440 cm^{-1} with clear shoulders at around 2500 cm^{-1} and 2300 cm^{-1} in both the leading and trailing regions of the peak. The observed

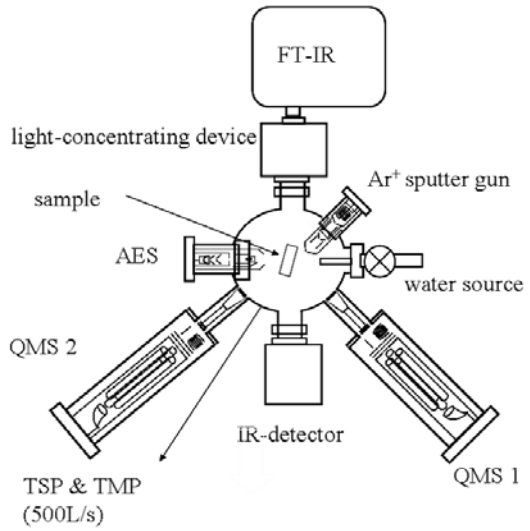

FIG. 1: Experimental apparatus: the main reaction chamber are equipped with Auger electron spectrometer AES, infrared absorption spectrometer FT-IR and IR-detector, quadrupole mass spectrometers QMS1 and QMS2, and titanium sublimation pump TSP and turbo-molecular pump TMP.

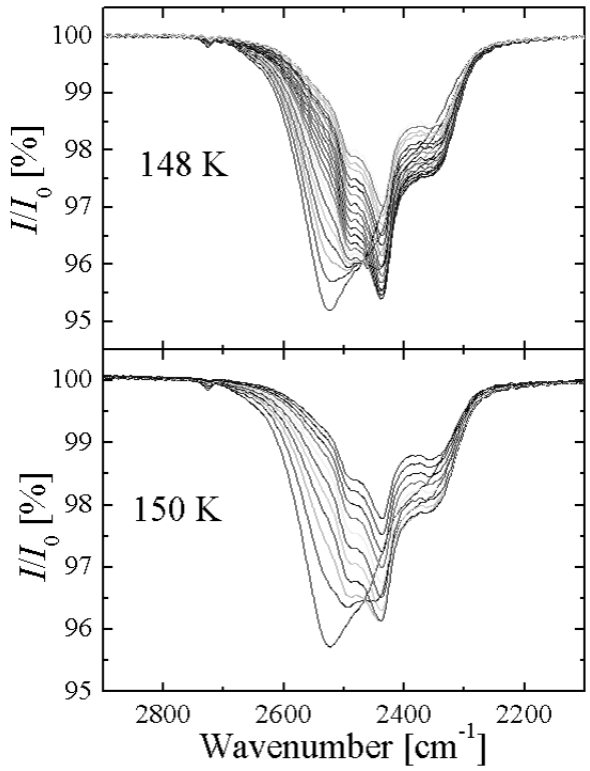

FIG. 2: Plots of IRAS spectra recorded during crystallization of ASW and subsequent sublimation of CI phases at 148 K(upper panel) and 150 K (lower panel).

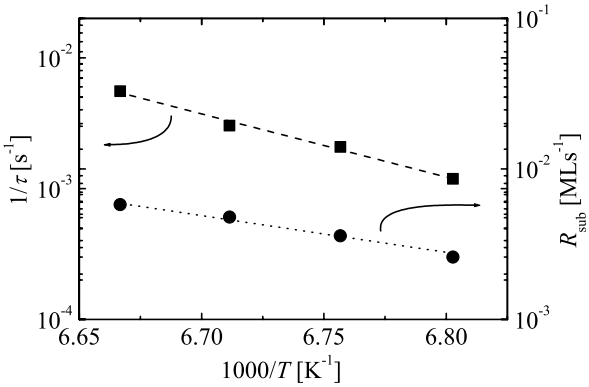

FIG. 3: Arrhenius-type plots of crystallization times τ and CI sublimation rates $R_{\rm sub}$.

maximum peak positions and line shapes of these IRAS spectra for the ASW and CI were in good agreement with those reported in the literature [13]. The D_2O layers deposited at 84 K were ASW, which persisted during settling time for the desired annealing temperatures. However, once the desired temperatures were reached at t=0, the IRAS measured spectra exhibited a gradual peak shift from ASW to CI with t. Figure 2 shows time evolutions of IRAS spectra recorded during annealing at 148 K (upper panel) and 150 K (lower panel). From such finger prints of the measured IRAS spectra we defined crystallization time τ when CI growth became complete. In Table I the measured crystallization times were summarized, and their Arrhenius plots were made in Fig. 3. From the plots the activation energy for the ASW crystallization, $E_{\rm a}$, was evaluated to be $E_{\rm a} = 0.95 \pm 0.03$ eV.

During the ASW crystallization, a burst of D_2O emission followed by a slow desorption was observed. This burst of molecular emission is due to sublimation of ASW. Figure 4 shows the time evolution of the desorbed D_2O molecules (upper panel) together with the mapped IRAS spectra (middle panel), and plots of the total area of of the IRAS spectra (lower panel) measured at 148 K. The intensity of the IRAS spectra of the converted CI decreased almost linearly, suggesting a zero-order sublimation [10]. These gross features

TABLE I: Film thickness L, Crystallization times τ, rates of CI sublimation $R_{\rm sub}$, crystallization rate constants $k_{\rm A}$, and dimensional orders n at annealing temperature T.

T [K]	L [ML]	τ [s]	$R_{\rm sub}$ [ML/s]	$k_{\rm A}[10^{-3}/{\rm s}]$	n
147	11	840	0.0026	2.1±0.8	1.88±0.10
148	8	480	0.0036	3.8±0.1	1.82±0.17
149	25	330	0.0048	7.0±1.3	1.96±0.06
150	8	180	0.0058	10.5±3.3	1.88±0.14

appeared in the time evolutions of the IRAS spectra and the D_2O emission are in good agreement with those reported by Kondo et al. [14] studied from the regime of ASW as thick as 50 ML.

From the slope of the portion corresponding to such a zero-order sublimation as shown in Fig. 4, CI sublimation rate $R_{\rm sub}$ were evaluated. Results were summarized in Table I. Then their Arrhenius plot was made in Fig. 3 to determine activation energy for the CI sublimation, $E_{\rm sub}$. As a result, we obtained $E_{\rm sub} = 0.51\pm0.05$ eV. One may notice that this value is very close to the value of 0.56 eV measured in the sublimation of H_2O crystalline ice on Pt(111) [9].

In order to understand ASW crystallization kinetics in the thin film regime, the measured IRAS spectra were deconvoluted into ASW and CI components. In actual practice of deconvolution, the IRAS spectra were fit with a line shape function that consists of two reference IRAS spectra for ASW and CI. In obtaining best curve fits, intensities of the two reference curves were adjusted. Figure 5 shows an example of deconvoluted IRAS spectrum which was obtained at a midstage of annealing at 148 K (fourth curve in upper panel of Fig. 2). One should note that the measured IRAS spectrum can be nicely fit with the two reference spectra, i.e., no any additional components are neceaasry. As will be shown below this can be related to the CI growth mode in the thin film regime.

To more quantitatively understand the ASW crystallization kinetics, we calculated con-

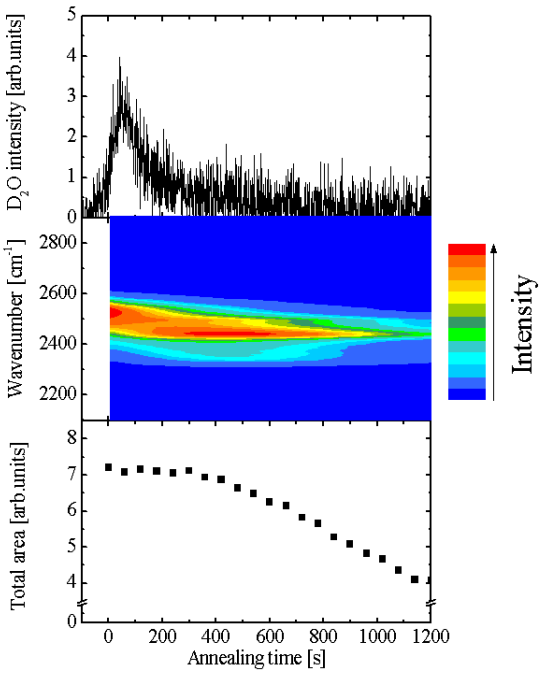

FIG. 4: Plots of desorbed D_2O intensity (upper), mapped IRAS spectra (middle), and yield of IRAS spectra (lower) as a function of annealing time t.

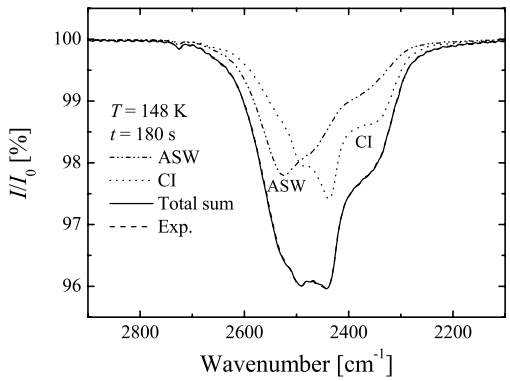

FIG. 5: Deconvolution of IRAS spectra into ASW and CI components. The measured spectrum is completely fit with two reference curves for ASW and CI.

verted CI fractions with respect to the total amount of ASW and CI, χ, from the deconvoluted spectra as shown in Fig.5. Results were plotted in Fig. 6 as a function of t. With increasing annealing temperature T, the ASW crystallization rate increases, suggesting it is activated by T. The experimental data plotted in Fig. 6 were fit with an Avrami equation

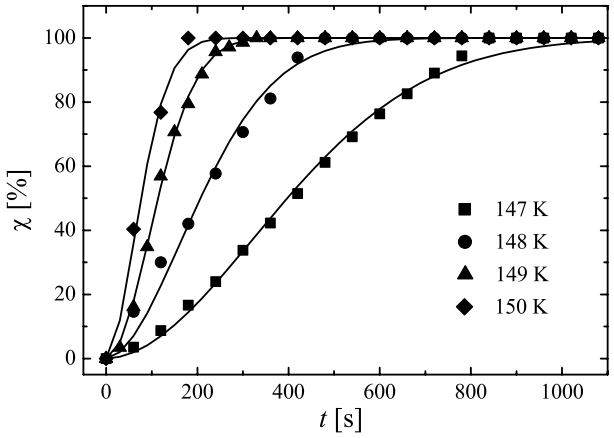

FIG. 6: Plots of measured χ and curve fits with the Avrami equation (solid lines).

[19, 20],

$$\chi = 1 - \exp(-(k_{\rm A}t)^n), \tag{1}$$

where $k_{\rm A}$ is the crystallization rate constant and n is the dimensional parameter relevant to CI growth. When the crystallization would follow one dimensional (1D) random nucleation and growth, we anticipate $n =\sim 2$, while when it would follow a three dimensional (3D) random nucleation and growth we anticipate $n =\sim 4$. From the best curve fits of the data with eq. (1) values of n were determined. Results were summarized in Table I. Note that the average value of n is very close to 2, which therefore suggests that the ASW crystallization proceeds along the 1D random nucleation and growth mode. This finding should be compared with the 3D random nucleation and growth generally recognized in the thick film regime. For ASW films as thick as 50 ML the influence of substrates to the crystallization may be small, and therefore the CI nucleation and growth proceed in the bulk of ASW layers. Smith et al. [7] found that the thickness dependence of ASW crystallization time is irrespective of substrates tested for hydrophilic Ru(001) and hydrophobic Au(111), suggesting that the influence of the first monolayer that wets the substrate [21] to the ASW

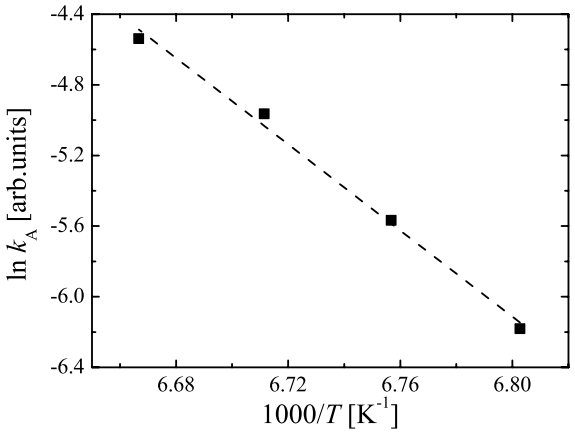

FIG. 7: Arrhenius plots of crystallization rate constant $k_{\rm A}$.

crystallization kinetics is rather small. This may not be at variance with the observation by Kimmel et al. [12] who found that crystalline ice films do not wet the first monolayer that wets Pt(111). Smith et al. [7] estimated the average distance (L^*) between CI nucleation embryos in ASW layers to be about 15 ML ($\sim$50 Å). Taking these observations into consideration, the 1D nucleation and growth observed in the thin film regime may not be simply interpreted in terms of the substrate effect on the crystallization. One should remind that our ASW films, except for the surface tested at 148 K, are thinner than L^*($\sim$15 ML). Therefore, one would expect that only one nucleation embryo grows in the lateral direction. No presence of boundary-layer water as noted in Fig. 5 may not be at variance with such a laterally restricted 1D growth mode.

Fitting the measured χ curves with Avrami equation (1) also determined the crystallization rate constants $k_{\rm A}$, which were summarized in Table I for the various temperatures examined. We made an Arrhenius plot of $k_{\rm A}$'s in Fig. 7, and then determined the activation energy for crystallization to be $E_{\rm A} = 1.01\pm0.05$ eV. This value is close to the apparent activation energy $E_{\rm a} = 0.95 \pm 0.03$ eV. The crystallization process predicted in the Avrami model is governed by nucleation rate constant $k_{\rm N}$ and growth rate constant $k_{\rm G}$. For the 1D

nucleation and growth, i.e., $n = 2$, we obtain $k_A^2 = k_N k_G$, which yields the energy relation $2E_A = E_N + E_G$, where E_N and E_G are the activation energies of nucleation and growth, relatively. In the present experiments neither of E_N nor E_G were separately determined. Kondo et al. [13] evaluated $E_N = 1.56$ eV and E_G=0.44 eV in the 3D nucleation and growth from the thick film regime on Ru(001). These values are close to those reported on Pt(111) [11, 22]. If the above values are taken for E_N and E_G, one can notice that the energy relationship $2E_A = E_N + E_G$ is satisfied with the presently obtained value E_A=1.01±0.05 eV. Thus it may be understood that the energetics of the ASW crystallization occurring near the substrate-ice interface is more or less the same to that in the bulk of thick ASW layers. In other words, although D_2O water wets the Ru substrate the ASW crystallization is not affected by the substrate even near the interface.

IV. CONCLUSION

The crystallization of amorphous solid water (ASW) and sublimation of the crystalline ice (CI) layers have been studied by means of IRAS and ITPD on the Ru(001) surface. Rates of conversion of ASW to CI were measured in the thin film regime of about 10 ML. From the analysis of CI conversion curves on the basis of the Avrami model we found that the one dimensional nucleation and growth of CI in the thin film regime is of the case. Thus the CI growth mode in the thin film regime is very much different from that in the thick film regime where a three dimensional nucleation and growth is generally operating. The activation energy for the ASW crystallization was evaluated to be about 1 eV which was not at variance with the activation energies for the nucleation and subsequent growth of CI evaluated in the thick film regime.

Acknowledgments

The authors express their sincere thanks to T. Kondo for giving them his IRAS data in evaluating thickness of ASW and CI phases. This work was financially supported by a Grant-in-Aid for Specially-promoted Research (No.17002011) and Young Scientists (B) (No.20740140) of the Ministry of Education, Culture, Sports, Science, and Technology of Japan.

---

[1] J. M. Greenberg, Surf. Sci. 500(2002)793.

[2] G. Manico, G. Raguni, V. Pirronello, J. E. Roser and G. Vidali, Astrphys. J. 548(2001), L253.

[3] T. E. Madey, R. E. Johnson, T. M. Orland, Surf. Sci. 500(2002)838.

[4] D. A. Williams, E. Herbst, Surf. Sci. 500(2002)823.

[5] P. Jenniskens and D. F. Blake, Astrophys. J. 473(1996)1104.

[6] J. H-Captain, G. A. Grieves, A. Alexandrov, M. T. Sieger, H. Chen and T. M. Orlando, Phys. Rev. B 72(2005)035431.

[7] R. S. Smith, C. Huang, E. K. L. Wong, and B. D. Kay, Surf. Sci. 367(1996)L13.

[8] P. Löfgren, P. Ahlström, D. V. Chakarov, J. Lausmaa, and B. Kasemo, Surf. Sci. 367(1996)L19.

[9] P. Löfgren, P. Ahlström, J. Lausma, B. Kasemo, and D. Chakarov, Langmuir, 19(2003)265.

[10] F. E. Livingston, J. A. Smith, S. M. George, Surf. Sci. 423(1999)145.

[11] Z. Dohnálek, G. A. Kimmel, R. L. Ciolli, K. P. Stevenson, R. C. Smith, B. D. Kay, J. Chem. Phys. 112(2000)5932.

[12] G. A. Kimmel, N. G. Petrik, Z. Dohnálek, B. D. Kay, J. Chem. Phys. 126(2007)114702.

[13] T. Kondo, H. S. Kato, M. Bonn, M. Kawai, J. Chem. Phys. 127(2007)094703.

[14] T. Kondo, H. S. Kato, M. Bonn and M. Kawai, J. Chem. Phys. 126(2007)181103.

[15] T. Kondo, H. S. Kato, M. Kawai and M. Bonn, Chem. Phys. Lett. 448(2007)121.

[16] E. H. G. Backus, M. Grecea, A. W. Kleyn, and M. Bonn, Phys. Rev. Lett. 92(2004)236101.

[17] A. Kouchi, J. Cryst. Growth, 99(1990)1220.

[18] P. Ahlström, P. Löfgren, J. Lausma, B. Kasemo, and D. Chakarov, Phys. Chem. Chem. Phys. 6(2004)1890.

[19] M. J. Avrami, J. Chem. Phys. 8(1941)212.

[20] R. H. Doremus, "Rates of Phase Transformations", (Academic, New York, 1985).

[21] S. Haq, C. Clay, G. R. Darling, G. Zimbitas, A. Hodgson, Phys. Rev. B 73(2006)115414.

[22] D. J. Safaric, C. B. Mullins, J. Chem. Phys. 121(2004)6003.

Figure captions

Fig.1 Experimental apparatus: the main reaction chamber are equipped with Auger electron spectrometer AES, infrared absorption spectrometer FT-IR and IR-detector, quadrupole mass spectrometers QMS1 and QMS2, and titanium sublimation pump TSP and turbo-molecular pump TMP.

Fig.2 Plots of IRAS spectra recorded during crystallization of ASW and subsequent sublimation of CI phases at 148 K(upper panel) and 150 K (lower panel).

Fig.3 Arrhenius-type plots of crystallization times τ and CI sublimation rates $R_{\rm sub}$.

Fig.4 Plots of desorbed D_2O intensity (upper), mapped IRAS spectra (middle), and yield of IRAS spectra (lower) as a function of annealing time t.

Fig.5 Deconvolution of IRAS spectra into ASW and CI components. The measured spectrum is completely fit with two reference curves for ASW and CI.

Fig.6 Plots of measured χ and curve fits with the Avrami equation (solid lines).

Fig.7 Arrhenius plots of crystallization rate constant $k_{\rm A}$.